Journal of Nanopores Systems

Original Research Paper

Synthesis of Zeolite/ZIF-8 Composite as a Catalyst for Aldol Condensation Reaction

Hadis Ghaedrahmat[1]

[1]*Department of Chemistry, Faculty of Science, Arak University, Arak 38156-8-8349, Iran;*

Article history
Received: 3 August 2024
Revised: 18 April 2025
Accepted: 29 April 2025

*Hadis Ghaedrahmat
Department of Chemistry, Faculty of Science, Arak University, Arak 38156-8-8349, Iran;
Email: hadis_ghaedrahmat@yahoo.com

Abstract: In this research work, two catalytic nanocomposites NaY Zeolite/Zn/Methyl Imidazole and NaY Zeolite/Methyl Imidazole/Zn were synthesized by two different chemical methods. The model used to prepare these nanocatalysts was the ship-in-a-bottle method. Each of the obtained catalysts were identified by various methods such as FT-IR, XRD, BET, FESEM, EDX, TGA and NH3-TPD. Preparation of catalyst with micro-meso structure with strong acid sites confirmed by BET and NH3-TPD techniques. The synthesis of this substance leads to the stabilization of the structure of ZIF-8 and increasing the chemical and physical stability of ZIF-8 in acidic environments. The obtained composites were used for the aldol condensation reaction of benzaldehyde derivatives 2-X and 4-X. The obtained results show that zeolite/ZIF-8 catalytic nanocomposites have high efficiency for organic reactions. NaY/Zn/Methyl Imidazole and NaY/Methyl Imidazole/Zn catalyst nanocomposites bring 96.7% and 96.2% efficiency for aldol condensation reactions, respectively. Achieving such high yields indicates the achievement of nano-catalysts that have been very efficient in promoting the organic reaction in question.

Keywords: ZIF-8, zeolite, composite, Aldol Condensation

Introduction

The aldol condensation reaction is a fundamental organic process that facilitates the formation of carbon-carbon (C-C) bonds between carbonyl compounds, typically aldehydes and ketones, to yield β-hydroxy carbonyl compounds (aldols) which can dehydrate to form α,β-unsaturated carbonyl [1]. This reaction is pivotal in the synthesis of various complex molecules, including biofuels, pharmaceuticals, and natural products [2].

Interestingly, the reaction's selectivity and efficiency can be influenced by several factors, such as the presence of water and acid in the feedstocks, which can affect the catalyst and the reaction outcome [3]. Additionally, the diffusion of reactants and products within the catalyst's pores plays a crucial role in determining the selectivity of the aldol condensation reaction [4]. Moreover, the reaction mechanism and the rate-limiting step, particularly in base-catalyzed aldol condensations, have been subjects of study, with findings suggesting the final loss of hydroxide and formation of the C=C bond as the rate-limiting step.

In summary, aldol condensation is a versatile and widely applied reaction in organic chemistry, essential for constructing C-C bonds and synthesizing diverse compounds with significant applications. The reaction's complexity and the factors affecting its selectivity and efficiency are critical considerations for optimizing conditions and designing catalysts for specific synthetic goals [5].

Aldol condensation is a fundamental organic reaction that forms carbon-carbon (C-C) bonds between carbonyl compounds, typically aldehydes and ketones, under basic or acidic conditions. This reaction is pivotal in synthetic organic chemistry due to its ability to create complex molecules with high selectivity and is widely applied in the synthesis of natural products, pharmaceuticals, and biofuels. The process involves the formation of an enolate or enol, which then adds to another carbonyl group, yielding β-hydroxy carbonyl

compounds (aldols) that can dehydrate to form α,β-unsaturated carbonyl compounds [6].

Interestingly, the aldol condensation reaction is not only significant in laboratory-scale syntheses but also has implications in green chemistry and industrial applications. Efforts to develop greener methods for aldol condensation have led to solventless procedures that align with the principles of green chemistry, reducing waste and improving atom economy. Moreover, the reaction has been adapted to tandem processes, such as the tandem aldol condensation/Diels-Alder sequence, which allows for the efficient synthesis of complex structures in a single pot. Additionally, the reaction's mechanism and kinetics have been studied to understand the rate-limiting steps and the influence of solvent effects [7].

In summary, aldol condensation is a versatile and essential reaction in organic chemistry, enabling the construction of diverse molecular architectures with significant applications in various fields. Its importance is underscored by continuous research into its mechanisms, the development of greener methodologies, and its integration into tandem reaction sequences for efficient synthesis [8].

The aldol condensation reaction, a key process for synthesizing liquid fuel precursors and chemicals, can be catalyzed by various types of catalysts, including acidic, basic, acid-base amphoteric, and ionic liquids. Basic catalysts are noted for their high conversion and yield, but they present challenges in separation from the product [9]. Acid-base amphoteric catalysts, such as boehmite, have demonstrated excellent activity and selectivity, and are environmentally friendly and reusable. Additionally, the synthesis method, such as hydrothermal or sol-gel, can influence the catalyst's performance in aldol condensation reactions [10].

Interestingly, the catalyst's structure and the presence of specific functional groups can significantly affect the reaction outcome. For instance, the presence of secondary amines grafted onto mesoporous silica has been shown to enhance catalytic activity due to the formation of optimized acid and base groups [11]. Zeolite catalysts are notable for their performance and potential for industrial applications. Future research should continue to explore the development of catalysts that combine high activity, selectivity, and ease of separation to advance the application of aldol condensation in producing valuable compounds [12, 13].

Experimental

Materials:

All chemicals used in this study were of analytical grade and purchased from Merck or Fluka, except where otherwise specified. NaY zeolite was obtained from SPAGE (Tehran, Iran). For the synthesis of ZIF-8, zinc nitrate hexahydrate ($Zn(NO_3)_2 \cdot 6H_2O$, 98%, Sigma-Aldrich) was used as the metal source, and 2-methylimidazole (mIm, 99%, Sigma-Aldrich) served as the organic linker.

X-ray powder diffraction (XRD) patterns were recorded using a Philips 1840 diffractometer equipped with Cu-Kα radiation at ambient temperature. Energy-dispersive X-ray spectroscopy (EDX) was performed using an Oxford X-Max system to analyze the elemental composition of the samples. Fourier-transform infrared (FT-IR) spectra were recorded using a Galaxy Series FT-IR 5000 spectrometer.

The textural properties were investigated using BET surface area analysis with a SIBATA apparatus (Model App 1100-SA), using nitrogen adsorption at 77 K. Additional BET measurements were carried out using ASAP 2020 V3.04 E, with nitrogen adsorption at −196.66 °C. Thermogravimetric and differential scanning calorimetry (TGA-DSC) analyses were conducted using a Diamond Pyris TG/DT 6300 instrument, from 30 to 1000 °C at a heating rate of 10 °C/min under air flow.

Morphological features were examined using a field-emission scanning electron microscope (FE-SEM; Zeiss Sigma-VP) and a transmission electron microscope (TEM; EM900, ZEISS). Additionally, microactivity profiling (MAP) and NH_3-temperature programmed desorption (NH_3-TPD) analyses were carried out to assess the catalytic activity and surface acidity of the synthesized materials.

Preparation of catalytic composite by Ship in Bottle method:

The first method:

To prepare the NaY/Zn/Methyl Imidazole nanocomposite, 1 g of NaY zeolite was dispersed in 5 mL of deionized water using an ultrasonic bath for 15 minutes to ensure uniform dispersion. Separately, a 0.1 M solution of zinc nitrate hexahydrate ($Zn(NO_3)_2 \cdot 6H_2O$) was prepared by dissolving the appropriate amount of salt in 50 mL of deionized water. This solution was then added to the zeolite suspension and the resulting mixture was stirred continuously at room temperature for 24 hours.

After stirring, the solid product was separated by filtration, washed thoroughly with distilled water, and dried at room temperature. The dried powder was subsequently redispersed in 5 mL of deionized water. Then, 8 mL of a 9.8 mmol solution of 2-methylimidazole in deionized water was added dropwise, and the mixture was subjected to reflux at 100 °C for 8 hours.

The final product, NaY/Zn/Methyl Imidazole, was collected by filtration, washed three times with deionized water, and dried. The obtained nanocomposite was then characterized using various analytical techniques.

The second method:

For synthesize the NaY/Methyl Imidazole/Zn nanocomposite, 1 g of NaY zeolite was initially dispersed in 5 mL of deionized water. Subsequently, 5.36 mmol of 2-methylimidazole, dissolved in 10 mL of deionized water, was added to the mixture. The resulting suspension was refluxed at 100 °C for 24 hours using a heat stirrer to promote interaction between the organic linker and the zeolite framework.

Following reflux, the precipitate was collected by filtration, washed three times with distilled water, and dried at room temperature. The dried product was then redispersed in deionized water using an ultrasonic bath for 15 minutes. Next, 1.34 mmol of zinc nitrate hexahydrate ($Zn(NO_3)_2 \cdot 6H_2O$), dissolved in 8 mL of deionized water, was added to the mixture and refluxed at 100 °C for an additional 8 hours.

The final product, NaY/Methyl Imidazole/Zn, was isolated by filtration, thoroughly washed with distilled water, and dried at room temperature. The synthesized nanocomposite was characterized using various analytical techniques [14, 15].

Investigation of Catalytic Activity: Aldol Condensation Reaction

To evaluate the catalytic performance of the synthesized nanocomposites, the aldol condensation reaction was selected as a model transformation. In a typical experiment, 0.33 mmol of cyclohexanone was mixed with 0.66 mmol of 4-X-benzaldehyde or 2-X-benzaldehyde (X = H, Me, Cl) derivatives in a 10 mL round-bottom flask. Subsequently, varying amounts of the synthesized catalysts NaY Zeolite/Zn/Methyl Imidazole and NaY Zeolite/Methyl Imidazole/Zn were added separately to the reaction mixtures.

The reactions were carried out under ambient conditions (room temperature) and stirred for an optimized period of time. Upon completion, the reaction mixtures were analyzed by determining the melting points of the products and by FT-IR spectroscopy to confirm the formation of aldol condensation products.

The nanocomposites NaY Zeolite/Zn/Methyl Imidazole and NaY Zeolite/Methyl Imidazole/Zn, synthesized according to Scheme 1, functioned as heterogeneous hybrid acid catalysts. Their catalytic efficiency was assessed based on product yield and selectivity under identical reaction conditions [16].

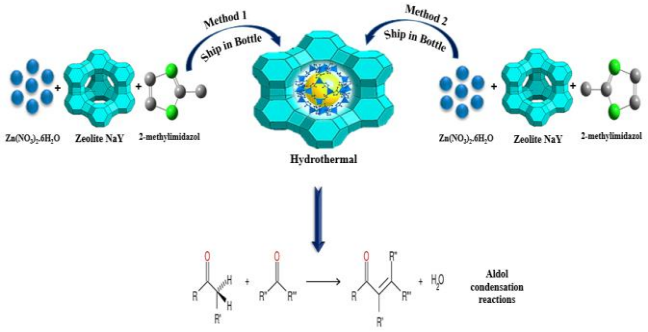

Scheme 1. for the preparation of NaY Zeolite/ZIF-8 catalytic composite

Results and discussion:

FT-IR spectra

T-IR spectroscopy was employed to characterize the chemical structure of pure ZIF-8, NaY zeolite, NaY Zeolite/Zn/Methyl Imidazole, and NaY Zeolite/Methyl Imidazole/Zn nanocomposites, as shown in Figure 1a–d. In Figure 1a, the absence of any absorption band around 1850.3 cm^{-1} confirms the formation of the imidazolate framework, indicating successful coordination between the zinc ions and 2-methylimidazole.

For ZIF-8, a characteristic absorption band appears at 1569 cm^{-1}, corresponding to the C=N stretching vibration of the imidazole ring. Additional bands observed at 1309.2 cm^{-1} and 1454.9 cm^{-1} are attributed to the stretching vibrations of the cyclic bonds within the imidazole ligand. Moreover, the absorption band near 756 cm^{-1} is associated with out-of-plane bending vibrations of the imidazole ring, further confirming the presence of the ZIF-8 framework.

These spectral features collectively validate the incorporation of ZIF-8 structures within the zeolite-based nanocomposites and demonstrate the successful functionalization of the NaY framework [17, 18]. In addition to the characteristic bands of the imidazole ring, the FT-IR spectra revealed key features supporting the structural integrity of both ZIF-8 and zeolite components in the nanocomposites. The band observed at 420.8 cm^{-1} is attributed to the Zn–N stretching vibration, indicating the coordination between Zn^{2+} ions and nitrogen atoms from the methyl imidazole ligand. The appearance of a similar band at 424 cm^{-1} further confirms the formation of Zn–N bonds, which are indicative of imidazolate linkage formation (Figure 1) [19]. For the NaY zeolite framework, the symmetric stretching vibration of the TO_4 unit (where T = Si or Al) appears prominently around 745.3 cm^{-1}, while the bending vibrations associated with the TO_4 units are observed in the range

of 440 cm^{-1} (Figure 1b). These characteristic zeolite bands remain visible in the composite materials, suggesting that the zeolite framework is preserved after the incorporation of ZIF-8 components [20].

The FT-IR spectra of NaY Zeolite/Zn/Methyl Imidazole and NaY Zeolite/Methyl Imidazole/Zn nanocomposites are presented in Figure 1c and 1d, respectively. The presence of broad and overlapping peaks in both spectra confirms the coexistence of characteristic bands from both the zeolite and ZIF-8 structures. All major absorption bands associated with the individual components—NaY zeolite and ZIF-8—are visible in the composite spectra, providing clear evidence for the formation of dual-phase nanocomposite catalysts.

Furthermore, broad peaks observed at 3467 cm^{-1} for NaY Zeolite/Zn/Methyl Imidazole and 3457cm^{-1} for NaY Zeolite/Methyl Imidazole/Zn correspond to the stretching vibrations of O–H groups. These peaks are slightly shifted to lower wavenumbers compared to those in the pure materials, which suggests the formation of hydrogen bonds between the hydroxyl groups of the zeolite surface and nitrogen atoms in the imidazole ligand of ZIF-8. This interaction likely contributes to enhanced structural integration and stability within the hybrid nanocomposites [21].

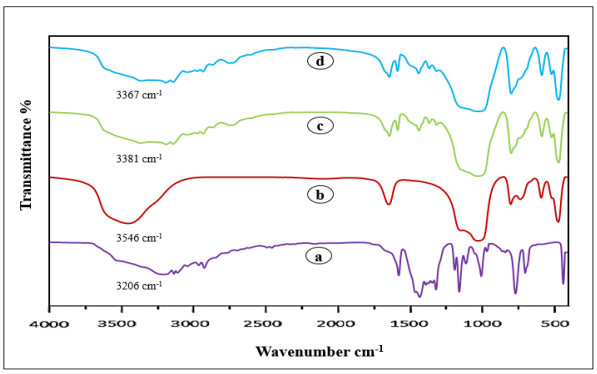

Fig. 1. FT-IR spectrum of pure ZIF-8 (a) NaY Zeolite (b), NaY zeolite/Zn/Methyl Imidazole (c), NaY zeolite/Methyl Imidazole/Zn (d)

X-ray Diffraction (XRD) Analysis

The XRD patterns of the synthesized nanocomposite catalysts NaY Zeolite/Zn/Methyl Imidazole (Figure 2a) and NaY Zeolite/Methyl Imidazole/Zn (Figure 2b) demonstrate the successful incorporation of ZIF-8 into the NaY zeolite framework. The diffraction peaks observed at 2θ values of 7.3°, 12.78°, 16.64°, 24.66°, 28.22°, and 33° correspond to the characteristic crystalline structure of ZIF-8, consistent with the standard JCPDS card no. 89-3739 [22,23], and are marked with red stars in the patterns.

Simultaneously, the patterns exhibit distinct peaks at 2θ = 6.3°, 15.6°, 23.7°, 27.2°, and 31.5°, which are attributed to the NaY zeolite framework and align well with JCPDS card no. 011-1829 [24,25], denoted by black circles. The presence of both sets of peaks in the XRD profiles of both nanocomposites confirms that the synthesis process preserved the crystallinity and structural integrity of both ZIF-8 and NaY zeolite phases.

A comparison of relative peak intensities reveals that, in both composites, the intensity of ZIF-8 peaks is slightly reduced compared to that of pure ZIF-8. This suggests partial encapsulation or surface dispersion of ZIF-8 within the porous matrix of the zeolite. However, the retention of sharp and well-defined peaks for both phases indicates that no significant phase transformation or structural degradation occurred during synthesis.

To further assess crystallinity, the average crystallite size of the ZIF-8 domains in the composites was estimated using the Scherrer equation:

$$D=K\lambda/\beta\cos\theta$$

Where,D is the crystallite size,K is the shape factor (typically 0.9),λ is the X-ray wavelength (Cu Kα = 1.5406 Å),β is the full width at half maximum (FWHM) in radians and θ is the Bragg angle.

Using the most intense peak of ZIF-8 (at 2θ ≈ 7.3°), the calculated average crystallite size for ZIF-8 in both composites was found to be in the range of 22–28 nm, indicating the formation of nanoscale ZIF-8 domains. This nanoscale dispersion is advantageous for catalysis, as it increases surface area and the availability of active sites.

Overall, the XRD analysis confirms that both NaY Zeolite/Zn/Methyl Imidazole and NaY Zeolite/Methyl Imidazole/Zn composites consist of well-preserved crystalline structures of both ZIF-8 and NaY zeolite, forming a stable and hybridized catalytic framework.

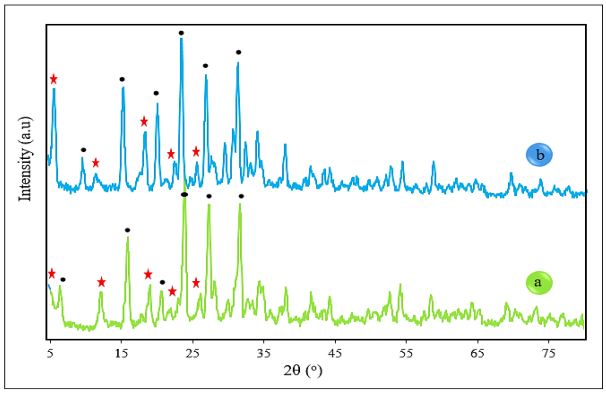

Fig. 2. XRD patterns for catalytic composites, NaY zeolite/Zn/Methyl Imidazole (a), NaY zeolite/Methyl Imidazole/Zn (b). Red stars for ZIF-8 and black circle for NaY.

Table 1. Elemental analysis (EDS) of synthesized catalysts

Element	Al	Si	O	C	N	Zn	Si/Al	C/N	C/Zn
NaY/Zn/Methyl Imidazole (W%)	16.62	46.79	20.97	7.95	5.03	2.64	2.81	1.58	3.01
NaY/Methyl Imidazole/Zn (W%)	17.01	48.33	16.56	9.30	5.74	3.06	2.84	1.62	3.04

SEM, EDX, and Elemental Mapping Analysis

The morphology of the synthesized nanocomposites NaY Zeolite/Zn/Methyl Imidazole and NaY Zeolite/Methyl Imidazole/Zn was examined using scanning electron microscopy (SEM), as illustrated in Figure 3a, b and 3d, e, respectively. The SEM images reveal that ZIF-8 particles exhibit a predominantly spherical morphology with particle sizes ranging from approximately 60 to 90 nm, closely associated with the larger NaY zeolite crystals [26–28]. The observation of surface cracks on the composite particles suggests the development of a mesoporous structure within the catalysts, which is consistent with previous reports [20].

Energy-dispersive X-ray spectroscopy (EDX) analysis was performed to confirm the elemental composition of the nanocomposites. Figures 3c and 3f present the EDX spectra for NaY Zeolite/Zn/Methyl Imidazole and NaY Zeolite/Methyl Imidazole/Zn, respectively, confirming the presence of Si, Al, C, N, and Zn elements in both catalysts. The quantitative elemental compositions are summarized in Table 1. Notably, the Si/Al ratio in the NaY zeolite component is approximately 2.8, corroborating the successful incorporation of the NaY framework as reported in the literature [29].

Furthermore, elemental mapping (MAP) analyses were conducted to investigate the spatial distribution of key elements. As shown in Figure 4a and 4b, carbon (C), nitrogen (N), and zinc (Zn) are uniformly dispersed throughout the catalyst matrices. This homogeneous distribution supports the effective integration of the ZIF-8 phase within the NaY zeolite framework and suggests consistent active site availability across the nanocomposite catalysts.

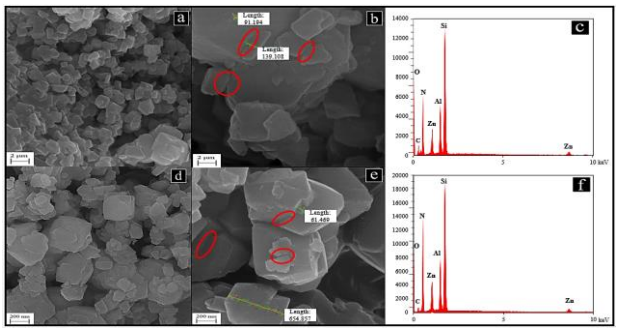

Fig. 3. FESEM morphology and EDX spectra for NaY zeolite/Zn/Methyl Imidazole (a, b, c), NaY zeolite/Methyl Imidazole/Zn (d, e, f) catalysts

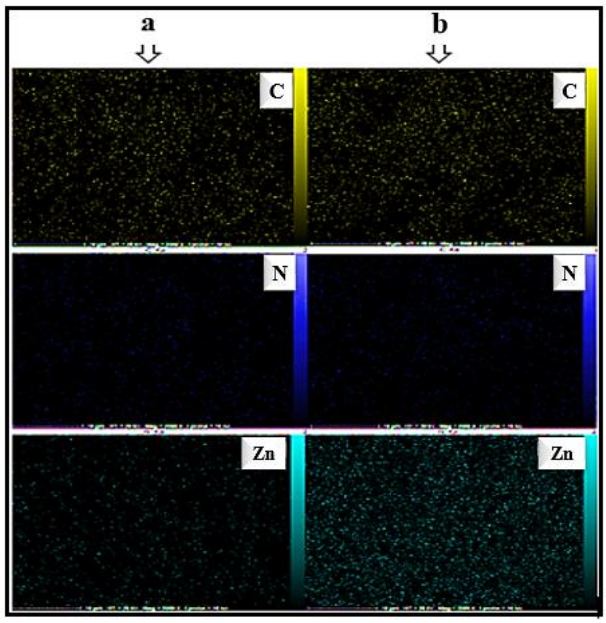

Fig. 4. Elemental mapping of C, N, and Zn for NaY zeolite/Zn/Methyl Imidazole (a) and NaY zeolite/Methyl Imidazole/Zn (b)

TGA-DTA Analysis

Thermogravimetric analysis (TGA) and differential thermal analysis (DTA) were performed under nitrogen atmosphere to evaluate the thermal stability of the synthesized catalysts. The results are presented in

Figure 5. For the NaY Zeolite/Zn/Methyl Imidazole catalyst (Figure 5A), a total weight loss of 14.50% was observed. The initial weight loss occurred between 40 and 130 °C and is attributed to the removal of adsorbed and physically bound water molecules. The second significant weight loss took place in the temperature range of 290 to 490 °C, corresponding to the decomposition of organic components within the catalyst. This stage is also accompanied by weak exothermic peaks in the DTA curve at approximately 200, 260, and 490 °C, indicating the gradual degradation of organic moieties. In contrast, the NaY Zeolite/Methyl Imidazole/Zn catalyst (Figure 5B) exhibited a single major weight loss between 30 and 180 °C, attributed primarily to the removal of both chemically and physically adsorbed water. The DTA curve similarly shows weak exothermic peaks around 200, 260, and 490 °C, associated with water removal and partial decomposition of organic bonds. Overall, these thermal analyses suggest that the hybrid catalytic composites, derived from the combination of pure ZIF-8 and NaY zeolite, possess enhanced thermal stability. The lower and more gradual weight loss indicates that the nanocomposite structures remain intact over a wide temperature range, confirming their suitability for catalytic applications under elevated temperatures [29, 31].

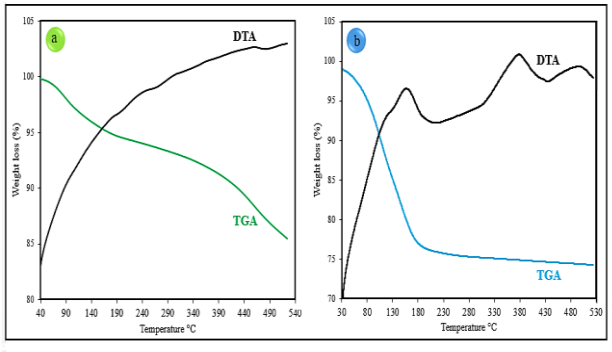

Fig. 5. TG-DTA and DTG patterns of NaY zeolite/Zn/Methyl Imidazole (a) and NaY zeolite/Methyl Imidazole/Zn (b)

Nitrogen adsorption-desorption

The nitrogen adsorption-desorption isotherms of the synthesized NaY Zeolite/Zn/Methyl Imidazole and NaY Zeolite/Methyl Imidazole/Zn nanocomposites are presented in Figures 6a and 6b, respectively. At low relative pressures ($P/P_0 < 0.1$), the isotherms indicate the presence of a microporous structure characteristic of both nanocomposites [32]. Furthermore, the observed Type IV isotherm with a pronounced hysteresis loop between $0.4 < P/P_0 < 0.9$ confirms the coexistence of mesoporous features in the materials, suggesting a hierarchical porous structure.

The porosity of both catalysts exhibits a combination of sheet-like, spherical, and cylindrical pore geometries, consistent with previous studies on similar composites [33]. The detailed textural parameters, including BET surface area, t-plot micropore volume, total pore volume, and average pore diameter, are summarized in Table 2 for pure NaY zeolite and the two synthesized nanocomposites.

A noticeable reduction in both surface area and pore volume is observed upon composite formation with ZIF-8, which can be attributed to partial pore blockage of the NaY zeolite by ZIF-8 crystals and the development of a new mesoporous phase on the catalyst surface [34, 35]. This structural modification is further supported by the Barrett-Joyner-Halenda (BJH) pore size distribution profiles shown in Figure 6b, which reveal two distinct pore size populations corresponding to the microporous and mesoporous domains in the nanocomposites [36].

These results indicate that the synthesized nanocomposites possess a well-developed hierarchical micro-mesoporous structure that is advantageous for catalytic applications, providing enhanced accessibility and diffusion of reactants.

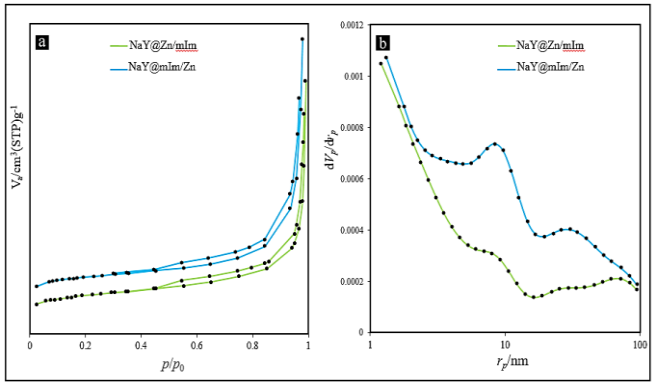

Fig. 6. The nitrogen absorption–desorption isotherms (a) and BJH plot (b) of NaY zeolite/Zn/Methyl Imidazole and NaY zeolite/Methyl Imidazole/Zn

Acidity measurement (NH_3-TPD)

Temperature-programmed desorption of ammonia (NH_3-TPD) was conducted to evaluate the acidity of the synthesized nanocomposites. Literature reports for pure ZIF-8 indicate two desorption peaks at approximately 70 °C and 220 °C, corresponding to weak acid sites. Similarly, pure NaY zeolite (Figure 7a) exhibits a relatively weak acidity peak centered around 196 °C. The NH_3-TPD profiles of both prepared catalysts revealed enhanced acidity compared to the pure zeolite. Both NaY Zeolite/Zn/Methyl Imidazole

and NaY Zeolite/Methyl Imidazole/Zn composites showed increased peak intensities near 200 °C, indicating an amplification of weak acid sites associated with NaY zeolite. Notably, the NaY Zeolite/Zn/Methyl Imidazole catalyst (Figure 7b) displayed two additional peaks at 597 °C and 729 °C, which correspond to moderate and strong acid sites, respectively. In contrast, the NaY Zeolite/Methyl Imidazole/Zn catalyst (Figure 7c) presented a new peak at 570 °C, attributed to moderate acidity. These observations confirm that incorporating ZIF-8 into the NaY zeolite framework enhances the overall acidity of the nanocomposites, particularly by introducing moderate and strong acid sites, which are beneficial for catalytic activity.

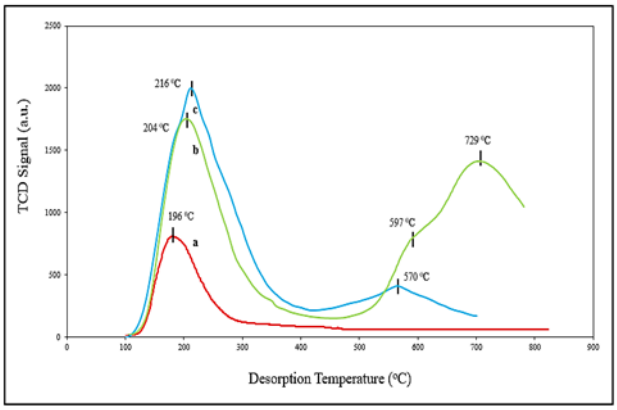

Fig. 7. The NH_3-TPD for pure NaY zeolite (a), NaY zeolite/Zn/Methyl Imidazole (b) and NaY zeolite/Methyl Imidazole/Zn (c)

Aldol condensation reactions

Aldol reactions are widely utilized for synthesizing β-hydroxy aldehydes, β-hydroxy ketones, and α, β-unsaturated aldehydes or ketones. These reactions proceed through addition or addition-elimination mechanisms involving aldehydes and ketones, forming carbon–carbon bonds that are fundamental in organic synthesis. The products, known as aldols, contain both aldehyde and alcohol functional groups, serving as important intermediates in the synthesis of various fine chemicals [37].

In this study, the aldol condensation between cyclohexanone and benzaldehyde derivatives was selected as a model reaction, particularly relevant to curcumin analog synthesis. To optimize the reaction yield, key parameters such as catalyst loading (entries 1–3, 10–12), temperature (entries 8, 9, 17, 18), and reaction time (entries 3–7, 13–16) were systematically investigated (Table 3). The results demonstrated that both NaY Zeolite/Zn/Methyl Imidazole and NaY Zeolite/Methyl Imidazole/Zn nanocomposites achieve optimal catalytic performance with 30 mg catalyst loading, a reaction time of 16 hours, and at room temperature [38, 39].

A notable finding was that the catalytic efficiency of pure NaY zeolite, ZIF-8, zeolite/Zn, and zeolite/2-methylimidazole individually was significantly lower compared to the synthesized nanocomposite catalysts.

This highlights the synergistic effect of the hybrid catalysts in promoting the aldol condensation.
Further catalytic tests using various benzaldehyde derivatives, including 2-hydroxybenzaldehyde, 2-chlorobenzaldehyde, 4-methylbenzaldehyde, and 4-methoxybenzaldehyde (entries 19–26), revealed a decline in efficiency with 2-X and 4-X substitutions. This reduction is attributed primarily to increased steric hindrance. Specifically, the diminished activity with 2-chlorobenzaldehyde is due to the electron-withdrawing effect of the chlorine substituent, which decreases the electrophilicity of the aldehyde carbon.

The proposed reaction mechanism for the aldol condensation to synthesize 2,6-di(benzylidene)cyclohexan-1-one is depicted in Scheme 2, based on previous studies [40]. The catalyst's acid-base sites facilitate the reaction through both acidic and basic pathways. Acidic sites activate benzaldehyde, promoting its condensation with cyclohexanone to form (E)-2-benzylidenecyclohexan-1-one. Concurrently, basic sites generate an enolate anion from cyclohexanone, which further reacts with benzaldehyde adsorbed on the catalyst. Subsequent dehydration completes the reaction, yielding the desired product 2-(2-methylbenzyl)-6-(2-methylbenzylidene) cyclohexanone (II) [40].

Optimum reaction conditions: cyclohexanone (1 mmol), 4-X-benzaldehyde (X = H, Cl) (2 mmol), reaction temperature (room temperature) and reaction time (16 h), Catalyst amount (30 mg)

Table 2. Calculation of micro-meso surface area and volume porous for pure NaY zeolite, NaY/Zn/Methyl Imidazole and NaY/Methyl Imidazole/Zn

Sample	S_{BET} m^2/g	S_{micro} m^2/g	S_{meso} m^2/g	V_t cm^3/g	V_{micro} cm^3/g	V_{meso} cm^3/g	d_{BJH} nm
NaY zeolite	530.30	522	8.30	0.50	0.45	0.05	1.25
NaY/Zn/Methyl Imidazole	109.08	10.13	98.95	0.0237	0.0024	0.0213	5.21
NaY/Methyl Imidazole /Zn	104.95	4.93	100.73	0.0248	0.0008	0.0240	7.99

Table 3. Aldol condensation reaction of cyclohexanone with benzaldehyde derivatives by synthetic catalysts.

Entry	Catalyst	Catalyst amount (mg)	Aldehyde	Time (h)	Temperature (°C)	Melting point (°C)	Yield (%)
1	NaY/Zn/mIm	15	benzaldehyde	16	room temperature	115	75.5
2		30	benzaldehyde	16	room temperature	116	96.7
3		60	benzaldehyde	16	room temperature	116	61.4
4		30	benzaldehyde	8	room temperature	116	48.6
5		30	benzaldehyde	10	room temperature	116	51.2
6		30	benzaldehyde	12	room temperature	116	69.2
7		30	benzaldehyde	14	room temperature	116	84.6
8		30	benzaldehyde	2	100	116	34.7
9		30	benzaldehyde	4	100	116	49.8
10	NaY/mIm/Zn	15	benzaldehyde	16	room temperature	116	80.8
11		30	benzaldehyde	16	room temperature	115	96.2
12		60	benzaldehyde	16	room temperature	116	68.2
13		30	benzaldehyde	8	room temperature	116	60.2
14		30	benzaldehyde	10	room temperature	116	66.4
15		30	benzaldehyde	12	room temperature	116	76.4
16		30	benzaldehyde	14	room temperature	116	89.7
17		30	benzaldehyde	2	100	116	46.8
18		30	benzaldehyde	4	100	116	58.2
19	NaY/Zn/mIm	30	2-hydroxybenzaldehyde	16	room temperature	296	63.7
20		30	2-chlorobenzaldehyde	16	room temperature	125	73.4
21		30	4-methylbenzaldehyde	16	room temperature	165	64.7
22		30	4-methoxybenzaldehyde	16	room temperature	145	70.5
23	NaY/mIm/Zn	30	2-hydroxybenzaldehyde	16	room temperature	296	66.9
24		30	2-chlorobenzaldehyde	16	room temperature	125	80.4
25		30	4-methylbenzaldehyde	16	room temperature	165	65.8
26		30	4-methoxybenzaldehyde	16	room temperature	145	74.7
27	NaY Zeolite	30	benzaldehyde	16	room temperature	116	41.1
28	ZIF-8	30	benzaldehyde	16	room temperature	116	18.9
29	Zeolite/Zn	30	benzaldehyde	16	room temperature	116	34.6
30	Zeolite/2-mIm	30	benzaldehyde	16	room temperature	116	39.3
31	No Catalyst	30	benzaldehyde	16	room temperature	116	6.5

Selected Spectroscopic Data

2,6-Di(benzylidene)cyclohexan-1-one:

- Catalyst NaY zeolite/Zn/Methyl Imidazole:

m.p. ~116 °C; FT-IR (KBr, cm^{-1}): 1498 (C=C), 1689 (C=O), 2895 (C–H aliphatic), 3021 (C–H aromatic) (entries 1–9)

- Catalyst NaY zeolite/Methyl Imidazole/Zn:

m.p. ~116 °C; FT-IR (KBr, cm^{-1}): 1589 (C=C), 1664 (C=O), 2798 (C–H aliphatic), 3093 (C–H aromatic) (entries 10–18)

(2E, 6E)-2,6-Bis(4-hydroxybenzylidene)-4-R-cyclohexanone:

- Catalyst NaY zeolite/Zn/Methyl Imidazole:

m.p. ~296 °C; FT-IR (KBr, cm^{-1}): 3328 (O–H stretching), 2987 (C–H stretching), 1608 (C=O stretching), 1612, 1486, 1487 (C=C stretching), 1389 (C–H deformation), 1304 (O–H deformation), 1257 (C–O stretching), 959, 940, 831, 776, 752 (C–H out-of-plane deformation) (entry 19)

- Catalyst NaY zeolite/Methyl Imidazole/Zn:

m.p. ~296 °C; FT-IR (KBr, cm^{-1}): 3398 (O–H stretching), 2904 (C–H stretching), 1663 (C=O stretching), 1551, 1468, 1447 (C=C stretching), 1380 (C–H deformation), 1269 (O–H deformation), 1201 (C–O stretching), 958, 932, 824, 769, 758 (C–H out-of-plane deformation) (entry 23)

(2E,6E)-2,6-Bis(2-chlorobenzylidene) cyclohexanone:

- Catalyst NaY zeolite/Zn/Methyl Imidazole:

m.p. ~125 °C; FT-IR (KBr, cm^{-1}): 3411 (=CH stretching), 2906 (aromatic C–H stretching), 1718 (C=O stretching), 1454 (aromatic C=C stretching), 1233 (C–O stretching), 746 (C–Cl stretching) (entry 20)

- Catalyst NaY zeolite/Methyl Imidazole/Zn:

m.p. ~125 °C; FT-IR (KBr, cm^{-1}): 3408 (=CH stretching), 2928 (aromatic C–H stretching), 1694 (C=O stretching), 1458 (aromatic C=C stretching), 1227 (C–O stretching), 743 (C–Cl stretching) (entry 24)

(2E, 6E)-2,6-Bis(4-methylbenzylidene) cyclohexanone:

- Catalyst NaY zeolite/Zn/Methyl Imidazole:

m.p. ~165 °C; FT-IR (KBr, cm^{-1}): 3414 (O–H), 2977 (CH_3), 2852 (C–H), 1657 (C=O), 1509 (-O-) (entry 21)

- Catalyst NaY zeolite/Methyl Imidazole/Zn:

m.p. ~165 °C; FT-IR (KBr, cm^{-1}): 3421 (O–H), 2989 (CH_3), 2813 (C–H), 1707 (C=O), 1502 (-O-) (entry 25)

(2E, 6E)-2,6-Bis(4-methoxybenzylidene) cyclohexanone:

- Catalyst NaY zeolite/Zn/Methyl Imidazole:

m.p. ~145 °C; FT-IR (KBr, cm^{-1}): 2988 (OCH_3), 2835 (C–H), 1702 (C=O), 1517 (-O-) (entry 22)

- Catalyst NaY zeolite/Methyl Imidazole/Zn:

m.p. ~145 °C; FT-IR (KBr, cm^{-1}): 2992 (OCH_3), 2823 (C–H), 1697 (C=O), 1515 (-O-) (entry 26) [20, 29].

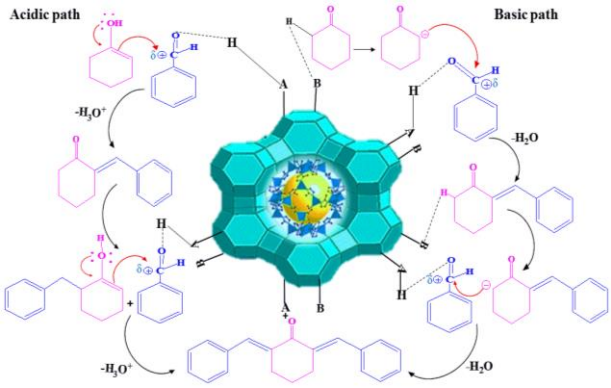

Scheme 2. Plausible mechanism for Crossed-Aldol condensation in the presence of catalytic composites synthesized as heterogeneous acid-base catalysts. acid (A) and base (B)

Catalyst recyclability

Another important aspect investigated in this research was the recyclability of the synthetic catalysts. The results demonstrated that both catalysts, NaY zeolite/Zn/Methyl Imidazole and NaY zeolite/Methyl Imidazole/Zn, can be reused effectively up to five cycles with only a minor decrease in catalytic efficiency.

The recycling procedure involved separating the catalyst from the reaction mixture by centrifugation at the end of each aldol condensation reaction. The recovered catalyst was then washed with ethanol, dried under vacuum, and reused in the subsequent reaction cycle.

As shown in Figure 8, the catalytic activity remained high across five reuse cycles, with only about a 10% reduction in efficiency observed by the fifth cycle. This indicates excellent stability and reusability of the catalysts under the reaction conditions.

Furthermore, characterization of the catalysts after five cycles by FT-IR spectroscopy and XRD analysis (Figures 9 and 10) revealed no significant changes in their structural integrity, confirming their robustness and suitability for repeated use [29, 41].

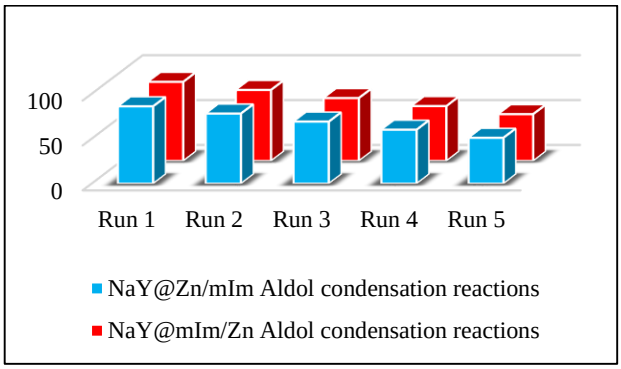

Fig. 8. Results of catalytic recovery of NaY zeolite/Zn/Methyl Imidazole and NaY zeolite /Methyl Imidazole/Zn

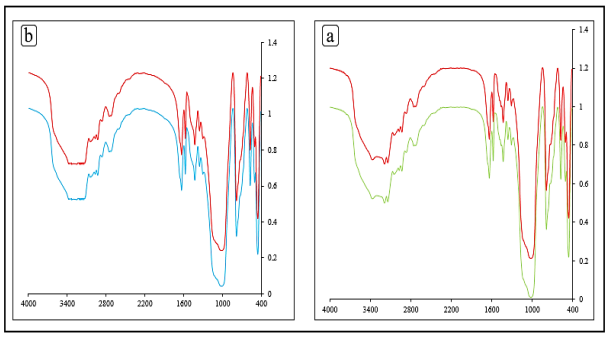

Fig. 9. FT-IR spectra of the catalysts as a fresh catalyst after 5 runs as catalysts for aldol condensation reactions for both NaY zeolite/Zn/Methyl Imidazole (a) and NaY zeolite/Methyl Imidazole/Zn (b) catalysts

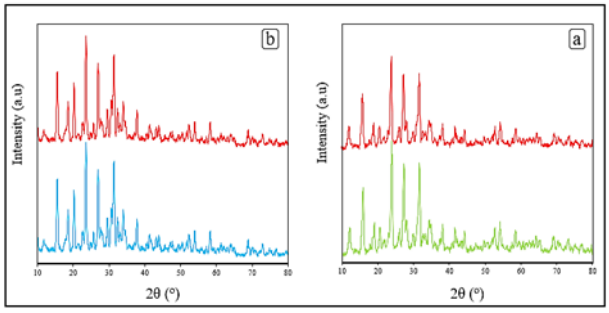

Fig. 10. XRD patterns of the catalysts as a fresh catalyst after 5 times of use as a catalyst for aldol condensation reactions for both NaY zeolite/Zn/Methyl Imidazole (a) and NaY zeolite/Methyl Imidazole/Zn (b) catalysts

Comparison with other works

To evaluate the performance and catalytic activity of the prepared NaY zeolite/Zn/Methyl Imidazole (a) and NaY zeolite/Methyl Imidazole/Zn nanocomposites, their efficiency in aldol condensation reactions was compared with that of various catalysts reported in the literature (Table 4). As shown, the catalysts synthesized in this study exhibit superior performance in terms of reaction temperature, time, and catalyst loading, achieving significantly higher yields than many previously reported catalysts. Another important advantage of these catalysts is their ease of separation from the reaction mixture, ensuring no contamination or residue remains in the final product. Additionally, their ability to be recycled multiple times without significant loss of activity, combined with their high acidity, makes these nanocomposites excellent candidates for aldol condensation reactions.

Table 4. Comparison of NaY Zeolite/ZIF-8 with other catalysts for the aldol condensation reaction

Catalyst	Catalyst amount	Time (h)	Temperature(°C)	Eter Yield%	Ref
Zn-MOF-74	40 mg	6	100	62	[42]
NaOH/TiO_2	0.15 g	3	25	72	[43]
Fe_3O_4@$Fe(OH)_3$	128 mg	20	50	38	[44]
ZnO	20 wt%	7	100	67	[45]
FAU/ZIF-8	0.25 g	6	130	67	[46]
Methanopyroline	10 mol%	1	50	91	[47]
NaY-C Zeolite	0.3 g	6	78	34.4	[48]
ZnS nanoparticles (NPs)	0.012 mmol	24	room temperature	77	[49]
SiO_2-Al_2O_3	10 mol%	45 min	70	85	[50]
$CoFe_2O_4$@Pr	0.05 g	2	70	91	[51]
In this work	30 mg	16	room temperature	95.6	

References

[1] Waldvogel, S. R. Comprehensive organic name reactions and reagents. ***Synthesis*** **2010**, *2010* (05), 892-892. BOOK REVIEW

[2] Choi, I.-H.; Hwang, J.; Han, J. W.; Hwang, K.-R. Carbon recovery from wasted aqueous-phase bio-oil to fuel precursors through aldol-condensation reaction: A comprehensive review. ***Journal of Industrial and Engineering Chemistry*** **2023**, 126, 115-126. https://doi.org/10.1016/j.jiec.2023.06.048

[3] Verma, A. K.; Kishor, B. N.; Prakash, O. Recent Advancement and Novel Application of Organocatalyzed Aldol Condensation Reactions: A Comprehensive

Review. ***Mini-Reviews in Organic Chemistry*** **2022**, *19* (6), 779-795. https://doi.org/10.2174/1570193X19666220104093837

[4] Huang, L.; Chen, D.; Liu, J.; Fu, H.; Yan, Z. Aldol condensation reaction in hierarchical ZSM-5 zeolite: a molecular dynamics simulation. ***Microporous and Mesoporous Materials*** **2023**, *348*, 112393. https://doi.org/10.1016/j.micromeso.2022.112393

[5] Kuei-Lin, C. The Complete Mechanism of an Aldol Condensation. **2016**.

[6] Nazari, A.; Heravi, M. M.; Zadsirjan, V. Oxazolidinones as chiral auxiliaries in asymmetric aldol reaction applied to natural products total synthesis. ***Journal of Organometallic Chemistry*** **2021**, *932*, 121629. https://doi.org/10.1016/j.jorganchem.2020.121629

[7] Robinson, T. M.; Box, M. C.; Gallardo-Williams, M. T. Choose your own (green) adventure: a solventless aldol condensation experiment for the organic chemistry laboratory. ***World J. Chem. Educ.*** **2020**, *8*, 104-106. DOI:10.12691/wjce-8-3-1

[8] Saeed Abaee, M.; Alizadeh, S.; Azadi, P.; Mojtahedi, M. M.; Halvagar, M. R. A Tandem Aldol Condensation/Diels-Alder Sequence of Reactions for One-Pot Synthesis of a New Series of Polysubstituted-Decalines. ***ChemistrySelect*** **2024**, *9* (5), e202304060. https://doi.org/10.1002/slct.202304060

[9] Zhang, X.; Li, Y.; Qian, C.; An, L.; Wang, W.; Li, X.; Shao, X.; Li, Z. Research progress of catalysts for aldol condensation of biomass based compounds. ***RSC advances*** **2023**, *13* (14), 9466-9478. DOI: 10.1039/D3RA00906H

[10] Reshma, P.; Vikneshvaran, S.; Velmathi, S. Boehmite—An Efficient and Recyclable Acid-Base Bifunctional Catalyst for Aldol Condensation Reaction. ***Journal of Nanoscience and Nanotechnology*** **2018**, *18* (6), 4270-4275. https://doi.org/10.1166/jnn.2018.15205

[11] Ma, Z.; Ma, X.; Liu, H.; He, Y.; Zhu, W.; Guo, X.; Liu, Z. A green route to methyl acrylate and acrylic acid by an aldol condensation reaction over H-ZSM-35 zeolite catalysts. ***Chemical communications*** **2017**, *53* (65), 9071-9074. https://doi.org/10.1039/C7CC04574C

[12] Xie, Y.; Sharma, K. K.; Anan, A.; Wang, G.; Biradar, A. V.; Asefa, T. Efficient solid-base catalysts for aldol reaction by optimizing the density and type of organoamine groups on nanoporous silica. ***Journal of catalysis*** **2009**, *265* (2), 131-140. https://doi.org/10.1016/j.jcat.2009.04.018

[13] Wang, J.; Li, H.; Xie, H.; Zu, L.; Shen, X.; Wang, W. Enantioselective Cascade Michael-Aldol Condensation Reaction. ***Synfacts*** **2008**, *2008* (01), 0095-0095. DOI: 10.1055/s-2007-991415

[14] Amooghin, A. E.; Sanaeepur, H.; Omidkhah, M.; Kargari, A. "Ship-in-a-bottle", a new synthesis strategy for preparing novel hybrid host–guest nanocomposites for highly selective membrane gas separation. ***Journal of Materials Chemistry A*** **2018**, *6* (4), 1751-1771. https://doi.org/10.1039/C7TA08081F

[15] Sun, T.; Xu, S.; Xiao, D.; Liu, Z.; Li, G.; Zheng, A.; Liu, W.; Xu, Z.; Cao, Y.; Guo, Q. Water-Induced Structural Dynamic Process in Molecular Sieves under Mild Hydrothermal Conditions: Ship-in-a-Bottle Strategy for Acidity Identification and Catalyst Modification. ***Angewandte Chemie International Edition*** **2020**, *59* (46), 20672-20681. https://doi.org/10.1002/anie.202009648

[16] Juneau, M.; Liu, R.; Peng, Y.; Malge, A.; Ma, Z.; Porosoff, M. D. Characterization of metal-zeolite composite catalysts: determining the environment of the active phase. ***ChemCatChem*** **2020**, *12* (7), 1826-1852. https://doi.org/10.1002/cctc.201902039

[17] TA DN, N. H.; TRINH, B. Preparation of nano-ZIF-8 in methanol with high yield [J]. ***The Canadian Journal of Chemical Engineering*** **2018**, *96* (7), 1518-1531. https://doi.org/10.1002/cjce.23155

[18] Yao, J.; Chen, R.; Wang, K.; Wang, H. Direct synthesis of zeolitic imidazolate framework-8/chitosan composites in chitosan hydrogels. ***Microporous and Mesoporous Materials*** **2013**, *165*, 200-204. https://doi.org/10.1016/j.micromeso.2012.08.018

[19] Chen, B.; Zhu, Y.; Xia, Y. Controlled in situ synthesis of graphene oxide/zeolitic imidazolate framework composites with enhanced CO_2 uptake capacity. ***RSC Advances*** **2015**, *5* (39), 30464-30471. https://doi.org/10.1039/C5RA01183C

[20] Mortezaei, Z.; Zendehdel, M.; Bodaghifard, M. A. Synthesis and characterization of functionalized NaP Zeolite@$CoFe_2O_4$ hybrid materials: A micro–meso-structure catalyst for aldol condensation. ***Research on Chemical Intermediates*** **2020**, *46*, 2169-2193. https://doi.org/10.1007/s11164-020-04085-z

[21] Chakarova, K.; Hadjiivanov, K. H-bonding of zeolite hydroxyls with weak bases: FTIR study of CO and N_2 adsorption on HD-ZSM-5. ***The Journal of Physical Chemistry C*** **2011**, *115* (11), 4806-4817. https://doi.org/10.1021/jp111961g

[22] Xie, W.; Gao, C.; Li, J. Sustainable biodiesel production from low-quantity oils utilizing $H_6PV_3MoW_8O_{40}$ supported on magnetic Fe3O4/ZIF-8 composites. ***Renewable Energy*** **2021**, *168*, 927-937. https://doi.org/10.1016/j.renene.2020.12.129

[23] Jing, Y.; Wang, J.; Yu, B.; Lun, J.; Cheng, Y.; Xiong, B.; Lei, Q.; Yang, Y.; Chen, L.; Zhao, M. A MOF-derived ZIF-8@ $Zn_{1-x}Ni_xO$ photocatalyst with enhanced photocatalytic activity. ***RSC Advances*** **2017**, *7* (67), 42030-42035. DOI: 10.1039/C7RA08763B

[24] Du, L.; Ding, S.; Li, Z.; Lv, E.; Lu, J.; Ding, J. Transesterification of castor oil to biodiesel using NaY zeolite-supported La_2O_3 catalysts. ***Energy Conversion and Management*** **2018**, *173*, 728-734. https://doi.org/10.1016/j.enconman.2018.07.053

[25] Yu, Y.; Mandizadeh, S.; Zhang, H.; Salavati-Niasari, M. The role of ZnO in reactive desulfurization of diesel over ZnO@ Zeolite Y: Classification, preparation, and evaluation. ***Separation and Purification Technology*** **2021**, *256*, 117784. https://doi.org/10.1016/j.seppur.2020.117784

[26] Jiang, M.; Cao, X.; Liu, P.; Zhang, T.; Zhang, J. ZIF-8@ polyvinylpyrrolidone nanocomposites based N-doped porous carbon for highly efficient oxygen reduction reaction in alkaline solution. ***Journal of The Electrochemical Society*** **2016**, *163* (6), H459. DOI 10.1149/2.1231606jes

[27] Thi Thanh, M.; Vinh Thien, T.; Thi Thanh Chau, V.; Dinh Du, P.; Phi Hung, N.; Quang Khieu, D. Synthesis of iron doped zeolite imidazolate framework-8 and its remazol deep black RGB dye adsorption ability. ***Journal of Chemistry*** **2017**, *2017*. https://doi.org/10.1155/2017/5045973

[28] Jiao, W. Q.; Fu, W. H.; Liang, X. M.; Wang, Y. M.; He, M.-Y. Preparation of hierarchically structured Y zeolite with low Si/Al ratio and its applications in acetalization reactions. ***RSC advances*** **2014**, *4* (102), 58596-58607. https://doi.org/10.1039/C4RA11042K

[29] Zendehdel, M.; Zamani, F.; Khanmohamadi, H. Immobilized 4-methyl-2, 6-diformyl phenol complexes on a zeolite: Characterization and catalytic applications in esterification, Diels–Alder and aldol condensation. ***Microporous and Mesoporous Materials*** **2016**, *225*, 552-563. https://doi.org/10.1016/j.micromeso.2016.01.042

[30] Mortezaei, Z.; Zendehdel, M.; Bodaghifard, M. A. Cu complex grafted on the porous materials: synthesis, characterization and comparison of their antibacterial activity with nano-Cu/NaY zeolite. ***Journal of the Iranian Chemical Society*** **2020**, *17*, 283-295. https://doi.org/10.1007/s13738-019-01769-1

[31] Mobinikhaledi, A.; Zendehdel, M.; Safari, P. Synthesis and characterization of some novel transition metal Schiff base complexes encapsulated in zeolite Y: effective catalysts for the selective oxidation of benzyl alcohol. ***Reaction Kinetics, Mechanisms and Catalysis***

2013, *110*, 497-514. https://doi.org/10.1007/s11144-013-0609-7

[32] Ghaedrahmat, H.; Masoomi, M. Y.; Zendehdel, M. Synthesize and characterization of ZIF-8/NaP zeolite composites as a stable acid-base catalyst for organic reactions. ***Polyhedron*** **2023**, *236*, 116372. https://doi.org/10.1016/j.poly.2023.116372

[33] Ta, D. N.; Nguyen, H. K.; Trinh, B. X.; Le, Q. T.; Ta, H. N.; Nguyen, H. T. Preparation of nano-ZIF-8 in methanol with high yield. ***The Canadian Journal of Chemical Engineering*** **2018**, *96* (7), 1518-1531. https://doi.org/10.1002/cjce.23155

[34] Zendehdel, M.; Khaghaninejad, S.; Tavakoli, F.; Ganji, S. Immobilized ionic liquid on the zeolite: its characterization and catalytic activity in the synthesis of coumarins via Pechmann reaction. ***Journal of the Iranian Chemical Society*** **2020**, *17*, 2555-2565. https://doi.org/10.1007/s13738-020-01950-x

[35] Chirra, S.; Wang, L.-F.; Aggarwal, H.; Tsai, M.-F.; Soorian, S. S.; Siliveri, S.; Goskula, S.; Gujjula, S. R.; Narayanan, V. Rapid synthesis of a novel nano-crystalline mesoporous faujasite type metal-organic framework, ZIF-8 catalyst, its detailed characterization, and $NaBH_4$ assisted, enhanced catalytic Rhodamine B degradation. ***Materials Today Communications*** **2021**, *26*, 101993. https://doi.org/10.1016/j.mtcomm.2020.101993

[36] Rongchapo, W.; Keawkumay, C.; Osakoo, N.; Deekamwong, K.; Chanlek, N.; Prayoonpokarach, S.; Wittayakun, J. Comprehension of paraquat adsorption on faujasite zeolite X and Y in sodium form. ***Adsorption Science & Technology*** **2018**, *36* (1-2), 684-693. https://doi.org/10.1177/0263617417715394

[37] Rao, K. K.; Gravelle, M.; Valente, J. S.; Figueras, F. Activation of Mg–Al hydrotalcite catalysts for aldol condensation reactions. ***Journal of Catalysis*** **1998**, *173* (1), 115-121. https://doi.org/10.1006/jcat.1997.1878

[38] Ghaedrahmat, H., Masoomi, M. Y., & Zendehdel, M. Synthesis and characterization of NaY@ ZIF‐8 composite by the ship‐in‐bottle method as a catalyst for esterification and transesterification reactions. ***Biofuels, Bioproducts and Biorefining, 2024,*** 18(5), 1175-1189. https://doi.org/10.1002/bbb.2605

[39] Ghaedrahmat, H., Masoomi, M. Y., & Zendehdel, M. Synthesis and characterization of Faujasite/ZIF-8 Composite by One-Pot Method, used as a Catalyst for Esterification and Aldol Condensation reaction. Catalysis Surveys from Asia, 2024, 28(1), 58-73. https://doi.org/10.1007/s10563-023-09417-8

[40] Mukaiyama, T. The directed aldol reaction. ***Organic reactions*** **2004**, *28*, 203-331. https://doi.org/10.1002/0471264180.or028.03

[41] Roy, A. S.; Poulose, A. C.; Bakandritsos, A.; Varma, R. S.; Otyepka, M. 2D graphene derivatives as heterogeneous catalysts to produce biofuels via esterification and trans-esterification reactions. ***Applied Materials Today*** **2021**, *23*, 101053. https://doi.org/10.1016/j.apmt.2021.101053

[42] Gäumann, P., Rohrbach, T., Artiglia, L., Ongari, D., Smit, B., van Bokhoven, J. A., & Ranocchiari, M. Tandem Hydroformylation‐Aldol Condensation Reaction Enabled by Zn‐MOF‐74. ***Chemistry–A European Journal 2023,*** 29(38), e202300939. https://doi.org/10.1002/chem.202300939

[43] Zhao, X.; Li, S.; Hu, Y.; Zhang, X.; Chen, L.; Wang, C.; Ma, L.; Zhang, Q. Synthesis of long chain alkanes via aldol condensation over modified chitosan catalyst and subsequent hydrodeoxygenation. ***Chemical Engineering Journal*** **2022**, *428*, 131368. https://doi.org/10.1016/j.cej.2021.131368

[44] Niu, F.; Zhang, L.; Luo, S.-Z.; Song, W.-G. Room temperature aldol reactions using magnetic Fe_3O_4@

$Fe(OH)_3$ composite microspheres in hydrogen bond catalysis. ***Chemical communications*** **2010**, *46* (7), 1109-1111. https://doi.org/10.1039/B920009F

[45] Vrbková, E., Kovářová, T., Vyskočilová, E., & Červený, L. Heterogeneous catalysts in the aldol condensation of heptanal with cyclopentanone. ***Progress in Reaction Kinetics and Mechanism, 2020,*** 45, 1468678319825713. https://doi.org/10.1177/1468678319825713

[46] Suttipat, D., Wannapakdee, W., Yutthalekha, T., Ittisanronnachai, S., Ungpittagul, T., Phomphrai, K., ... & Wattanakit, C. Hierarchical FAU/ZIF-8 hybrid materials as highly efficient acid–base catalysts for aldol condensation. ***ACS Applied Materials & Interfaces, 2018,*** 10(19), 16358-16366. https://doi.org/10.1021/acsami.8b00389

[47] Yu, H.; Xu, P.; He, H.; Zhu, J.; Lin, H.; Han, S. Highly enantioselective Biginelli reactions using methanopyroline/thiourea–based dual organocatalyst systems: asymmetric synthesis of 4-substituted unsaturated aryl dihydropyrimidines. ***Tetrahedron: Asymmetry*** **2017**, *28* (2), 257-265. https://doi.org/10.1016/j.tetasy.2016.11.015

[48] Liu, B., Xie, K., Oh, S. C., Sun, D., Fang, Y., & Xi, H. Direct synthesis of hierarchical USY zeolite for retardation of catalyst deactivation. ***Chemical Engineering Science, 2016,*** 153, 374-381. https://doi.org/10.1016/j.ces.2016.07.041

[49] Shah, E.; Soni, H. P. Inducing chirality on ZnS nanoparticles for asymmetric aldol condensation reactions. ***RSC advances*** **2013**, *3* (38), 17453-17461. https://doi.org/10.1039/C3RA41285G

[50] Bui, T. V.; Sooknoi, T.; Resasco, D. E. Simultaneous upgrading of furanics and phenolics through hydroxyalkylation/aldol condensation reactions. ***ChemSusChem*** **2017**, *10* (7), 1631-1639. https://doi.org/10.1002/cssc.201601251

[51] Tamoradi, T.; Mousavi, S. M.; Mohammadi, M. Praseodymium (iii) anchored on $CoFe_2O_4$ MNPs: an efficient heterogeneous magnetic nanocatalyst for one-pot, multi-component domino synthesis of polyhydroquinoline and 2, 3-dihydroquinazolin-4 (1 H)-one derivatives. ***New Journal of Chemistry*** **2020**, *44* (7), 3012-3020. https://doi.org/10.1039/C9NJ05468E